The Astrophysical Journal, 947:17 (10pp), 2023 April 10 https://doi.org/10.3847/1538-4357/acacfd

Investigating the Dominant Environmental Quenching Process in UVCANDELS/COSMOS Groups

Maxwell Kuschel[1], Claudia Scarlata[1], Vihang Mehta[2], Harry I. Teplitz[3], Marc Rafelski[4,5], Xin Wang[2], Ben Sunnquist[4], Laura Prichard[4], Norman Grogin[4], Anton Koekemoer[4], Rogier Windhorst[6], Michael Rutkowski[7], Anahita Alavi[2], Nima Chartab[8], Christopher J. Conselice[9], Y. Sophia Dai[10], Eric Gawiser[11], Mauro Giavalisco[12], Pablo Arrabal Haro[13], Nimish Hathi[4], Rolf A. Jansen[6], Zhiyuan Ji[12], Ray A. Lucas[4], Kameswara Mantha[1], Bahram Mobasher[14], Robert W. O'Connell[15], Brant Robertson[16], Zahra Sattari[17], L. Y. Aaron Yung[18], Romeel Davé[19], Duilia DeMello[20], Mark Dickinson[13], Henry Ferguson[4], Steven L. Finkelstein[21], Matt Hayes[22], Justin Howell[2], Sugata Kaviraj[23], John W. Mackenty[4], and Brian Siana[14]

[1] Minnesota Institute of Astrophysics and School of Physics and Astronomy, University of Minnesota, Minneapolis, MN 55455, USA; kusch037@umn.edu
[2] IPAC/Caltech, Pasadena, CA 91125, USA
[3] IPAC, Mail Code 314-6, California Institute of Technology, 1200 E. California Boulevard, Pasadena CA 91125, USA
[4] Space Telescope Science Institute, Baltimore, MD 21218, USA
[5] Department of Physics and Astronomy, Johns Hopkins University, Baltimore, MD 21218, USA
[6] Arizona State University, Tempe, AZ 85281, USA
[7] Minnesota State University-Mankato, Mankato, MN 56001, USA
[8] The Observatories of the Carnegie Institution for Science, 813 Santa Barbara Street, Pasadena, CA 91101, USA
[9] University of Manchester, Manchester M13 9PL, UK
[10] Chinese Academy of Sciences South America Center for Astronomy (CASSACA), National Astronomical Observatories of China (NAOC), 20A Datun Road, Beijing, 100012, People's Republic of China
[11] Rutgers University, New Brunswick, NJ 08901, USA
[12] University of Massachusetts, Amherst, MA 01003, USA
[13] NSF's National Optical-Infrared Astronomy Research Laboratory, Tucson, AZ 85719, USA
[14] University of California, Riverside, CA 92521, USA
[15] University of Virginia, Charlottesville, VA 22903, USA
[16] University of California, Santa Cruz, Santa Cruz, CA 95064 USA
[17] Department of Physics and Astronomy, University of California, Riverside, 900 University Avenue, Riverside, CA 92521, USA
[18] NASA Goddard Space Flight Center, Greenbelt, MD 20771, USA
[19] Institute for Astronomy, University of Edinburgh, Royal Observatory, Blackford Hill, Edinburgh EH9 3HJ, UK
[20] The Catholic University of America, Washington, DC 20064, USA
[21] University of Texas, Austin, TX 78712, USA
[22] Stockholm University, Stockholm 114 19, Sweden
[23] University of Hertfordshire, Hertfordshire AL10 9AB, UK
Received 2022 May 24; revised 2022 November 4; accepted 2022 November 29; published 2023 April 12

Abstract

We explore how the fraction of quenched galaxies changes in groups of galaxies with respect to the distance to the center of the group, redshift, and stellar mass to determine the dominant process of environmental quenching in $0.2 < z < 0.8$ groups. We use new UV data from the UVCANDELS project in addition to existing multiband photometry to derive new galaxy physical properties of the group galaxies from the zCOSMOS 20 k group catalog. Limiting our analysis to a complete sample of $\log(M_*/M_\odot) > 10.56$ group galaxies, we find that the probability of being quenched increases slowly with decreasing redshift, diverging from the stagnant field galaxy population. A corresponding analysis on how the probability of being quenched increases with time within groups suggests that the dominant environmental quenching process is characterized by slow (∼Gyr) timescales. We find a quenching time of approximately $4.91^{+0.91}_{-1.47}$ Gyr, consistent with the slow processes of strangulation and delayed-then-rapid quenching although more data are needed to confirm this result.

Unified Astronomy Thesaurus concepts: Galaxy groups (597); Galaxy quenching (2040); Galaxy evolution (594)

1. Introduction

Star formation in a galaxy requires the cooling of HI gas that eventually collapses and forms stars (Jeans 1902; Oosterloo et al. 2001). As a galaxy consumes its cold gas content via star formation, it eventually leads to cessation of star formation if the cold gas reservoir is not replenished. Galaxies are both observed and predicted to be hosted in halos containing large amounts of warm/hot gas, where cold streams can funnel cold gas into galaxies, slowly fueling star formation over time (Lilly et al. 2013; Ford et al. 2016; Werk et al. 2016). Both in the local universe and out to redshifts $z \sim 2$, galaxies are observed to obey a bimodal distribution in their star formation rates (Peng et al. 2010; Brammer et al. 2011; Muzzin et al. 2013). Many galaxies are found to be star forming at rates according to the star formation rate–stellar mass (SFR–M_*) main sequence, meaning the extent of star formation is dependent on the galaxy stellar mass and redshift (Speagle et al. 2014). At all times, however, there exists a population of galaxies in which no new stars are being formed, having ceased all significant star formation at earlier times. These galaxies are typically referred to as quenched, quiescent, or passive

galaxies. Various mechanisms have been proposed to explain why a galaxy stops forming stars. These quenching mechanisms could be internal to the galaxies themselves (Martig et al. 2009; Murray et al. 2011; He et al. 2019) or be the result of interactions between galaxies and the environment in which they reside (Peng et al. 2010; Presotto et al. 2012; Knobel et al. 2013; Wetzel et al. 2013; Wagner et al. 2016; Jian et al. 2017).

Large ($\log(M_*/M_\odot) > 12$) dark matter halos containing multiple subhalos of galaxies, known as the group and cluster environments, have been shown to influence star formation rates (SFRs) in both observations and hydrodynamical simulations (Wagner et al. 2016; Jian et al. 2017; Donnari et al. 2020). It is theorized that this occurs due to the large relative velocities that galaxies have, compared to the intracluster medium in groups and clusters (Gunn & Gott 1972; Larson et al. 1980). Furthermore, the group and cluster environments are more densely populated than the field, causing more interactions between galaxies in the form of dynamical friction and galactic mergers.

In this paper we investigate the role the group environment plays in determining a galaxy's probability of being quenched. In what follows, we will refer to "environmental quenching" as the ensemble of physical processes that affect the star formation rate in galaxies and are a consequence of the fact that a galaxy resides in a subhalo of a more massive halo. We will also work to separate the effects of environmental quenching from the quiescent population created due to internal processes driving quenching, known as "mass quenching," which significantly influences high-mass galaxies (Wetzel et al. 2013; Jian et al. 2017; Donnari et al. 2020).

Star formation is regulated, in part, by the interactions (gravitational and/or hydrodynamic) between the galaxies' gas and dark matter halo and/or gas content inside of the host halo. Tidal and ram-pressure stripping are very efficient quenching mechanisms, particularly in the cluster environment (McPartland et al. 2016). Ram-pressure stripping results from the relative motion of satellites (galaxies hosted together in a larger dark matter halo) inside a gas-rich halo (Gunn & Gott 1972), while tidal stripping is a consequence of various tidal forces acting on a satellite as it moves in the gravitational potential of the halo (Moore et al. 1996). These mechanisms are particularly efficient in very massive ($\log(M_*/M_\odot) > 14$), cluster-sized halos and on low-density galaxies but are also observed in smaller group-sized halos (Larson 1972; Jian et al. 2017).

Broadly speaking, two main paths are possible for the environmental quenching of star formation in satellites, which are characterized by the associated timescales. Ram-pressure stripping can influence star formation by directly removing the galaxy's cold gas (i.e., the interstellar medium) and stripping the outer, lower-density material (Gunn & Gott 1972). Ram-pressure stripping is an example of a rapid quenching process, working on timescales of a few million years (Taranu et al. 2014). Strangulation occurs when only the outer material is stripped, leaving the interstellar medium (ISM) gas untouched to continue forming stars for several billion years (Larson et al. 1980). Because much of the ISM is still in place, this process is much slower than ram-pressure stripping, quenching on timescales of $\sim$3 Gyr (Kawata & Mulchaey 2008).

We attempt to disentangle the relative importance of fast and slow quenching mechanisms by investigating the probability that a galaxy is quenched as a function of the time it has been in a group.

We focus on galaxy groups identified in the CANDELS/COSMOS field (Section 2), using the stellar population properties derived from the new UVCANDELS data set (X. Wang et al. 2023, in preparation; Section 2). We detail our methods of analysis in Section 3 and present our results in Section 4. Comparison with other studies is presented in Section 5, followed by our conclusion in Section 6. Throughout the paper, we assume a standard ΛCDM cosmology with parameters $H_0 = 68.8\,\mathrm{km\,s^{-1}\,Mpc^{-1}}$, $\Omega_M = 0.315$, and $\Omega_\Lambda = 0.685$ (Planck Collaboration et al. 2020; Gray et al. 2022); all magnitudes are expressed in the AB system (Oke 1974), and where applicable, we use the Chabrier initial mass function (IMF; Chabrier 2003).

2. The Data

In this work we study the fraction of quenched galaxies in groups and in the field. We derive new estimates of the galaxy physical properties using data from the recently completed UVCANDELS Hubble Treasury program (X. Wang et al. 2023, in preparation; Grogin et al. 2011; Koekemoer et al. 2011; Section 2.1). For the groups analysis we start from the galaxy groups identified in the *z*COSMOS 20 k group catalog of Knobel et al. (2012, hereafter, K12; Section 2.2).

2.1. UVCANDELS Catalog

The area of COSMOS covered with the Hubble Space Telescope (HST) optical and near-infrared observations by the CANDELS program (Grogin et al. 2011; Koekemoer et al. 2011) was one of the targets for follow-up F275W WFC3/UVIS and F435W Advanced Camera for Surveys/Wide Field Camera (ACS/WFC) observations with the recent UVCANDELS program, which covers four of the five CANDELS fields (COSMOS, GOODS-N, GOODS-S, AEGIS; PI: H. Teplitz; Cycle 26 GO 15647, F275W mosaics are currently available at the Mikulski Archive for Space Telescopes.[24] The addition of the observed UV and blue optical *B* band is particularly important for increasing the accuracy of the photometric redshifts used in this analysis (Rafelski et al. 2015).

The physical parameters we use in our analysis are derived by fitting the spectral energy distributions (SEDs) of our sample, obtained using the new F275W and F435W filters in addition to existing photometry (presented in further detail in V. Mehta et al. 2023, in preparation). The existing photometry that we use includes the HST/ACS F606W and F814W bands as well as the HST/WFC3 F125W and F160W bands available from Nayyeri et al. (2017). We also include the photometry from CFHT/MegaPrime $u^\star$, $g^\star$, $r^\star$, $i^\star$, and $z^\star$; the Subaru/SuprimeCam *B*, g^+, *V*, r^+, i^+ and z^+; VLT/VISTA *Y*, *J*, *H*, and *K*; Mayall/NEWFIRM *J*1, *J*2, *J*3, *H*1, *H*2, and *K*; as well as Spitzer/IRAC ch. 1, 2, 3, and 4 bands that are also available as part of the Nayyeri et al. (2017) catalog. The combination of these filters allows for a robust SED fitting, even for galaxies where some filters may be missing, such as some galaxies on the edge of the CANDELS/COSMOS field.

The stellar physical properties used for the analysis presented in this work are computed using CIGALE (Code Investigating GALaxy Emission; Burgarella et al. 2005; Noll

[24] doi:10.17909/8s31-f778

et al. 2009; Boquien et al. 2019). The full description of the SED-fitting procedure for the UVCANDELS catalog will be presented in a future publication (V. Mehta et al. 2023, in preparation). Briefly, we use Bruzual & Charlot (2003) stellar population models when fitting with a Chabrier (2003) IMF. We allow stellar metallicity to be a free parameter varying between $Z = 0.005$ and 2.5 Zsol. We choose the modified Charlot & Fall (2000) dust law to parameterize the dust and allow it to vary as a free parameter between $A_{V,\mathrm{ISM}} = 0$ and 4 with an $A_{V,\mathrm{ISM}}/A_{V,\mathrm{stellar}} = 0.44$. The stellar formation histories are parameterized as a delayed exponential with e-folding time varied over a grid between 30 Myr and 30 Gyr. Additionally, we allow for the possibility of an episode of recent starburst as a 10 Myr old burst with an exponential e-folding time of 50 Myr, and the contribution of the star formation (SF) burst is parameterized by the fraction of total mass generated in the burst. When spectroscopic redshifts are available, we did not find a significant difference between the physical properties derived with and without the UV and *B*-band data. When fitting for group galaxies from K12, we use the group redshifts provided by K12 to match the redshifts used in group identification. These were taken to be the median redshift of the group members, derived from the zCOSMOS survey (Lilly et al. 2009).

For the field galaxies in our sample we use photometric redshifts that have been computed with the inclusion of the new UVCANDELS F275W and F435W photometry, which combines redshifts in probability space from multiple redshift codes yielding robust redshifts. (B. Sunnquist et al. 2023, in preparation). When fitting, we add in quadrature a nominal error of 0.02 mag to all photometry in order to account for calibration variance across the various filters.

2.2. Selection of Group Galaxy Sample

In this work, we rely on the *z*COSMOS 20 k group catalog presented in K12. K12 use accurate spectroscopic redshifts from the *z*COSMOS catalog of Lilly et al. (2009) to identify group galaxies using two common group-finding algorithms, friends-of-friends (Huchra & Geller 1982; Eke et al. 2004; Berlind et al. 2006) and the Voronoi–Delaunay method (Knobel et al. 2009). These algorithms were calibrated using simulated mock galaxy catalogs extracted from the Millennium I Dark Matter N-Body simulation (Springel et al. 2005) by Kitzbichler & White (2007). The mock catalogs were used to fine-tune the parameters of the group identification algorithms in order to reach a completeness and purity of $\gtrsim$80% for groups with three or more members. From this K12 catalog we also use the derived group halo masses and group halo radii. These radii and masses were derived utilizing their mock catalogs by defining a probability distribution based on redshift, number of members, projected radius, and velocity dispersion and then matching this to their observed counterparts. For more information on how these physical properties were found, as well as their potential error, please see Section 4.2 of K12. For group centers they used a method based on weighting each group member by a Voronoi–Delaunay tessellation, described in Section 4.1 in Presotto et al. (2012).

Here we limit the analysis to groups in the area covered by the UVCANDELS data in the COSMOS field. In order for a group to be considered "covered" in the UVCANDELS area, we require that the projected size of the group, taken to be 1.5 times the group radius, falls within the CANDELS/COSMOS field. This selection does include eight galaxies that have been analyzed in UVCANDELS but were not covered by any UV filters. We have found that excluding these galaxies does not significantly change our results, so we have opted to include them. K12 defined the probability of a group being real, GRP2, based off of whether the group was found using both group-finding algorithms they employed. We only consider groups with GRP2 = 1.0 to ensure we are only looking at groups that confidently exist. We only consider groups with at least three spectroscopic members to ensure high values of completeness and purity described in K12. The K12 catalog also reports a probability for a galaxy to belong to its host group, computed from the redshift difference and projected distance between the galaxy and the group center. In the analysis below, we only include galaxies that have a probability $\geqslant$0.8. Richness was calculated using group members that had a probability of $\geqslant$0.8 of being in the group and was given an upper inclusive limit of 25 members to avoid contaminating our group sample with cluster galaxies. These cuts yield a 22-group sample across the $0.2 < z < 0.8$ redshift range within the CANDELS/COSMOS field (Figure 1).

2.3. Color and Mass Complete Sample

In order to ensure that we have a complete unbiased mass sample, we apply criteria based on redshift, magnitude, and stellar mass. Ideally, a volume-limited sample constructed by selecting all galaxies brighter than a rest-frame luminosity would ensure that we are comparing the same objects at all redshifts (e.g., Presotto et al. 2012). A typical choice in the literature is to use the evolution-corrected rest-frame *B*-band luminosity. The K12 group catalog inherits the selection function of the parent *z*COSMOS catalog that includes all galaxies with I_{F814W} magnitude brighter than 22.5. The I_{F814W} filter samples the rest-frame *B* band at $z \sim 0.8$; therefore, at this redshift the completeness of a *B*-band-selected catalog does not depend on galaxy colors. The resulting catalog, however, would still be affected by strong mass-dependent biases as old galaxies of a given stellar mass would preferentially be excluded compared to young galaxies of the same stellar mass, given their higher M/L ratio. Additionally, at redshifts higher (lower) than 0.8, a pure rest-frame *B*-band luminosity selection would preferentially exclude red (blue) galaxies, introducing additional mass-dependent biases in the final sample. In order to limit these effects, we follow Presotto et al. (2012) and define a luminosity- and mass-limited sample of group and field galaxies as follows.

First, we use an evolving *B*-band luminosity cut, assuming the luminosity evolution from Zucca et al. (2009), where $M^*_{\mathrm{Bev}} = -20.3 - 5\log(h_{70}) - 1.1z$. This corresponds to a cutoff in *B*-band absolute magnitude of $M_{B,\mathrm{cutoff}} = M^*_{\mathrm{Bev}} + 0.8$, which we apply for our sample. The derived mass cut follows the same approach as in Iovino et al. (2010), resulting in a mass cut of $\log(M_{\mathrm{cutoff}}/M_{\odot}) = 10.56$. More details on the methods used to derive the mass and luminosity cuts can be found in Presotto et al. (2012; Section 5.1). The final volume mass-limited sample of group galaxies includes 19 galaxies in 8 groups in the $0.2 \leqslant z < 0.45$ redshift range and 34 galaxies in 12 groups in the $0.45 \leqslant z < 0.8$ redshift range, notably removing two entire groups from our sample.

The comparison sample of field galaxies was selected from the UVCANDELS catalog, applying the same redshift, magnitude, and mass cut as for the group galaxy sample.

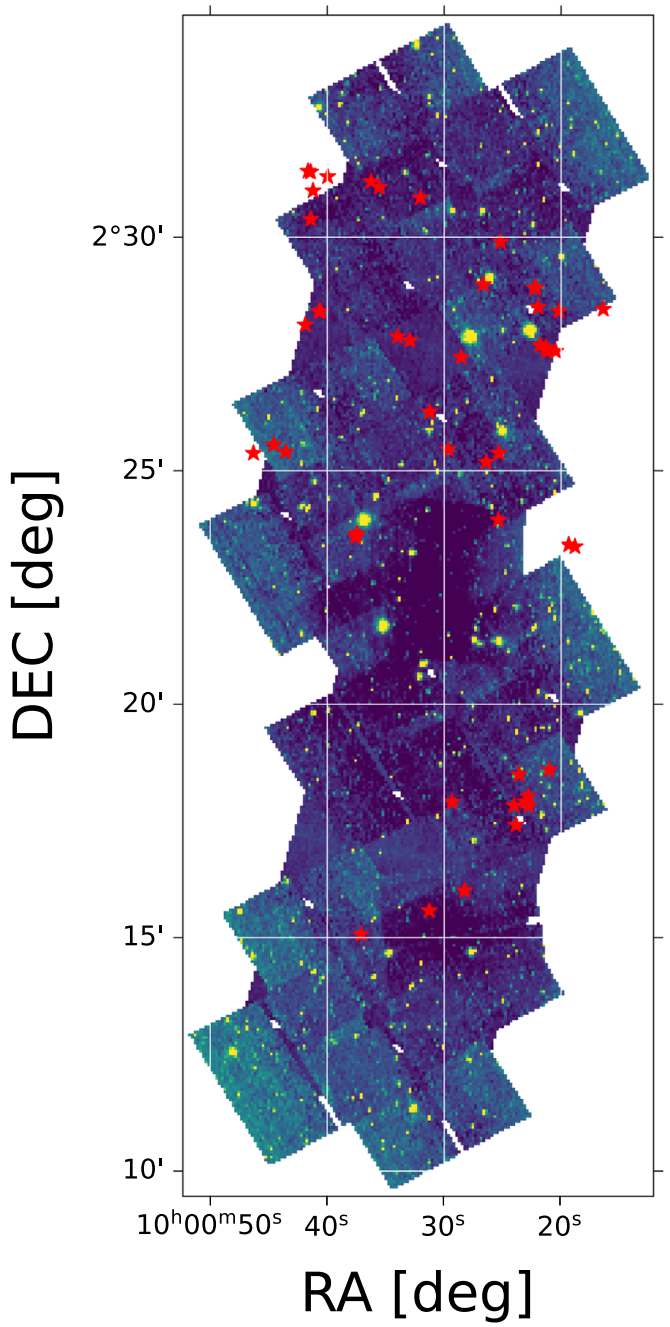

Figure 1. A plot of F275W and F435W mosaics overlaid with the group members being used. All group members have been reprocessed in UVCANDELS as described in Section 2.1, but not all are covered by the F275W or F435W mosaics.

Additionally this field sample was selected to only include galaxies that were detected in the F275W or F435W filters, which cover the UV at these redshifts. These cuts result in 33 and 87 field galaxies in the low- and high-redshift ranges, respectively.

3. Analysis

3.1. Selection of Quenched Galaxies

The criterion used to separate quenched from star-forming galaxies can influence the quenched fraction, particularly at the high-mass end ($\log(M_*) \gtrsim 10^{10.5} M_\odot$). Donnari et al. (2021) demonstrated that there is overall agreement among various definitions below this threshold. For larger stellar masses, however, different criteria for the identification of passive galaxies results in quenched fractions that can vary between 50% and 100%, depending on whether galaxies are centrals or satellites. We discuss why we use the *UVJ* method and why we believe this minimizes the cross contamination of the star-forming and quiescent populations in Section 5.

Here we proceed to use a rest-frame color selection to identify quenched galaxies based on their position in the rest frame $U-V$ versus rest frame $V-J$ diagram (e.g., hereafter, *UVJ* diagram; Williams et al. 2009; Whitaker et al. 2015; Martis et al. 2016). We use a *UVJ* color selection because it minimizes contamination from dusty star-forming galaxies. Classifying the data into star-forming and quiescent is necessary not only to analyze the impact of environmental quenching but also to compare our results to those found in the literature. The *UVJ* classification has been shown to provide a robust sample of star-forming and quiescent galaxies, minimizing the contamination of either sample (Williams et al. 2009; Brammer et al. 2011; Whitaker et al. 2011).

Figure 2 shows the *UVJ* diagram for galaxies both in groups and in the field. The rest-frame colors were computed from the best-fit models of the UVCANDELS data derived with CIGALE (V. Mehta et al. 2023, in preparation) using the Johnson U, V, and J bandpasses. Galaxies are color coded according to their specific star-formation rate (sSFR; SFR/M_*), as shown in the color bar on the right-hand side of the figure. Quiescent galaxies lie in the cloud on the top left of the distribution on both panels, with a lower sSFR that is commonly associated with quiescence (Williams et al. 2009; Whitaker et al. 2012; Speagle et al. 2014). We apply a cut to separate the quiescent galaxies from star-forming galaxies based on the bimodality of the distribution of colors following the method introduced by Williams et al. (2009). We first apply a cut to all galaxies with $(U-V) > 1.3$[25] that visually separates the populations of star-forming and quenched galaxies. We use the field galaxy population as the large number of galaxies makes the bimodality of the color distribution more prominent. For each galaxy, we compute the normal distance (in the *UVJ* plane) to the diagonal dividing line and plot the histogram of the distances in Figure 3. The final parameters (intercept and slope) of the separating line are determined with an iterative method. First, we adjust the slope of the cut to maximize the bimodality in Figure 3, and then we modify the intercept of the line to lie at the minimum between the two peaks. This method converged within two iterations, resulting in the definition of a quiescent galaxy:

$$(U-V) \geqslant 0.8(V-J) + 0.9;$$
$$(U-V) > 1.33. \quad (1)$$

This cut is in general agreement with the literature values reported by Williams et al. (2009) and Whitaker et al. (2015). Our cut is slightly higher; Williams et al. (2009) reports a slope of 0.88 and intercept of 0.69, while Whitaker et al. (2015) uses a slope of 0.8 and intercept of 0.7. These discrepancies are likely due to differences in the bandpass definition used to compute the $U-V$ and $V-J$ rest-frame colors in our analysis compared to others in the literature. Note that we do not consider a redshift-dependent selection of quiescent galaxies.

[25] This cut is applied to remove possible contamination by blue star-forming galaxies.

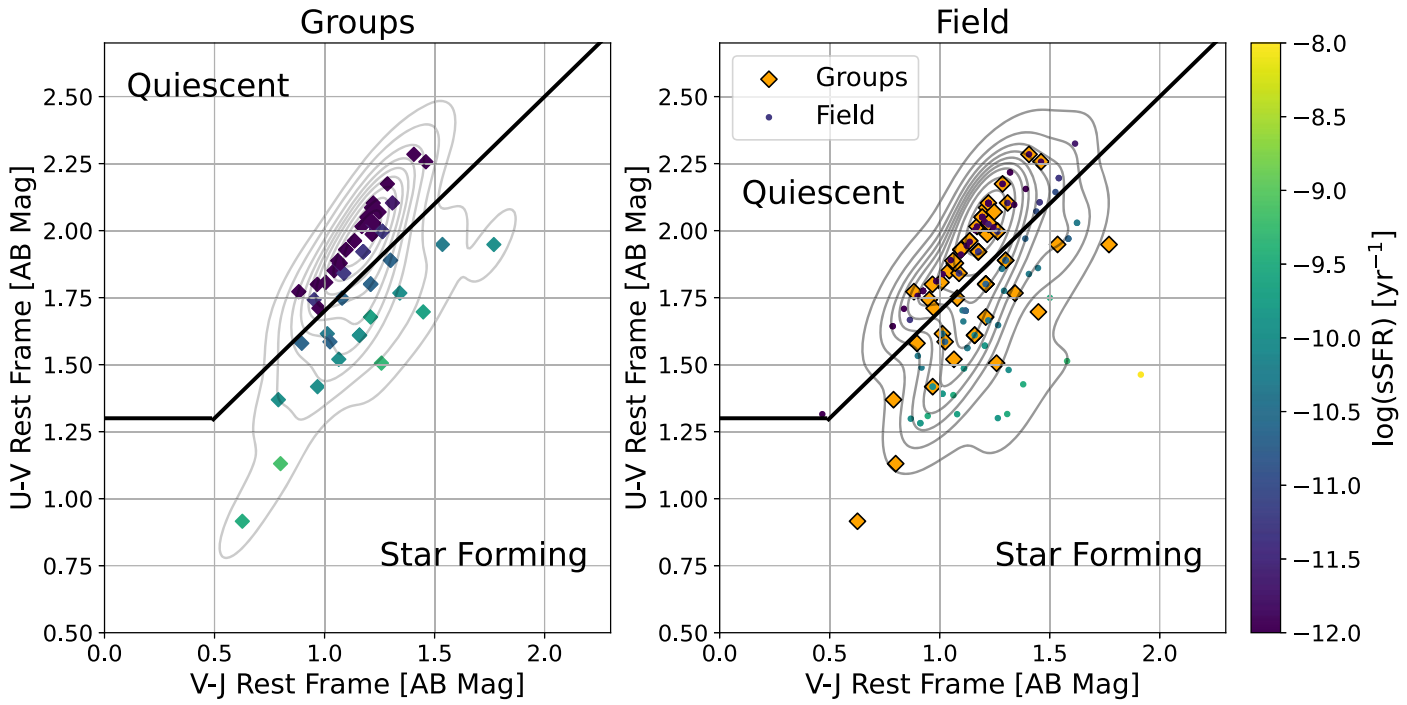

Figure 2. The *UVJ* diagram used to select the quiescent and star-forming galaxies. The line indicates the cut used to separate quiescent and star-forming galaxies as described in Section 3.1. The colors indicate the log(sSFR) in both the left and right panels. In the left panel we show the group galaxies after the mass and luminosity cuts. The right panel shows the field galaxies from the UVCANDELS COSMOS data set that are above the $M_{\rm cutoff} = 10.56$ mass cut and the absolute B-band magnitude $M_B < -19.5–1.1z$ cut and within the $0.2 < z < 0.8$ range. Overlaid on the right-hand side are the group galaxies in orange diamonds. Contour lines are based on the density of galaxies in the *UVJ* plot.

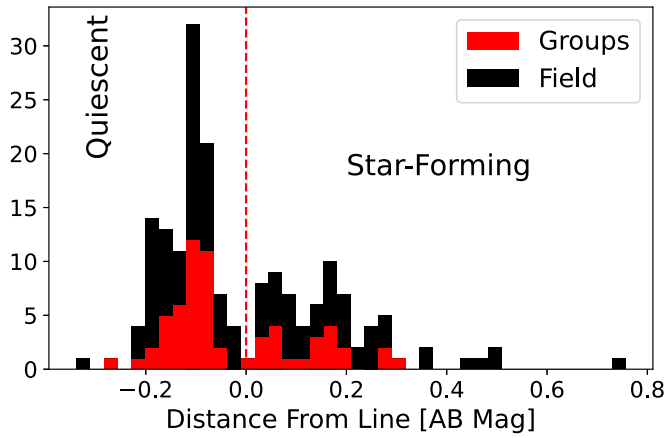

Figure 3. Histogram of distances to the *UVJ* cut, in AB Mag. The vertical dashed line indicates the *UVJ* cut that is used to select quiescent galaxies, created through an iterative process described in Section 3.1 Negative values are quiescent; positive values are star forming. Distances were only calculated for galaxies with $U - V > 1.3$.

Williams et al. (2009) find that the $U - V$ color for passive galaxies evolves by less than 0.15 mag out to $z \sim 2$, and thus, this effect is negligible in the redshift range considered here. The log(sSFR), indicated by the color, of the galaxies in Figure 2 confirms that in the selected region the majority of galaxies have low sSFR ($\log(\mathrm{sSFR}) < -11$) associated with quenched systems.

3.2. The Quenched Fraction

In the following we compute the probability of a galaxy being quenched, f_Q and $\widehat{f_Q}$. When calculating how the probability of being quenched depends upon a given predictor (redshift, group–center distance, or stellar mass), we use a logistic regression model as it helps us avoid binning of the data. In using this model we assume that f_Q, the probability of being quenched, follows a logistic function, with the predictor as the input variable x:

$$f_Q = \frac{1}{1 + e^{-(bx+a)}}. \quad (2)$$

To compute the a and b parameters of this model, we utilize Bayes's theorem, implementing a Markov Chain Monte Carlo algorithm with the PYMC3 Python package (Salvatier et al. 2016), using a normal distribution with a mean of 0 and standard deviation of 10 for the priors on a and b. With 5000 steps and the NUTS sampler, we are able to find the maximum a posteriori for a and b, listed for our two models below. Due to the multivariate nature of logistic regression we were able to fit two models, one that takes redshift and stellar mass to derive the mass dependence and redshift evolution of f_Q and a second model that takes redshift, stellar mass, group halo mass and normalized distance to the group center, normalized by the radius of the group (Figures 4–6). The maximum a posteriori for this first model are $a = -9.03^{+8.7}_{-8.7}$, $b_z = -2.2^{+1.8}_{-1.8}$, and $b_{\log(M)} = 1.021^{+0.8}_{-0.8}$ for the group model and $a = -8.35^{+7.0}_{-6.9}$, $b_z = -0.35^{+1.1}_{-1.1}$, and $b_{\log(M)} = 0.81^{+0.64}_{-0.64}$ for the field model, where b_z is the slope for the redshift and b_{logM} is the slope for the stellar mass. The maximum a posteriori for the second model are $a = -0.38^{+9.9}_{-9.4}$, $b_z = 7.49^{+9.3}_{-9.4}$, $b_{\log M} = 3.32^{+1.9}_{-1.8}$, $b_r = {}^{+1.5}_{-1.5}$, and $b_{\rm GM} = -3.85^{+2.7}_{-2.76}$, where b_z is the slope for the redshift, b_r is the slope for the normalized radius, b_{logM} is the slope for the galaxy stellar mass, and $b_{\rm GM}$is the slope for the group halo mass. This second model is used to analyze the radial distribution of f_Q in Figure 5. For each model we marginalize over the variables not being plotted.

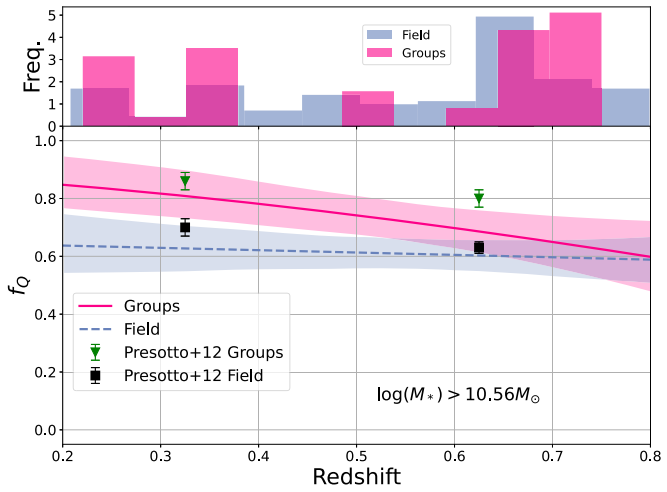

Figure 4. The probability of being quenched (f_Q) derived from a logistic regression model vs. the redshift of the galaxy. Only galaxies with $M_B < -19.5–1.1z$ and $\log(M_*/M_\odot) > 10.56$ are included. The red solid line corresponds to the logistic regression of the group galaxies, while the dashed blue line corresponds to the logistic regression of the field galaxies. The shaded regions correspond to the 68th percentile for each regression. Green upside-down triangles denote the field galaxies from Presotto et al. (2012), and black squares denote the group galaxies from Presotto et al. (2012). The gradual deviation of group galaxies from field galaxies suggests the group environment slowly changes the probability of galaxies being quenched, implying a slow quenching process is dominant in the group environment.

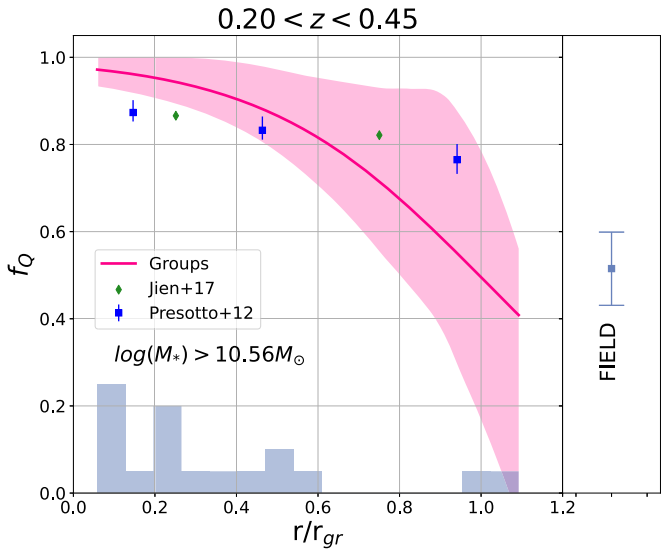

Figure 5. The probability of being quenched (f_Q) derived from a logistic regression model vs. the distance to the group center (r/r_{gr}) normalized by the radius of the group (r_{gr}). The histogram indicates the normalized distribution of group galaxies that went into constructing the model. The galaxies are limited to a redshift range of $0.2 < z < 0.45$, stellar mass of $\log(M_*/M_\odot) \geqslant 10.56$, and B-band absolute magnitude of $M_B < -19.5–1.1z$. The shaded regions correspond to the 68% interval of the regression model. The right-hand sidebar indicates $\widehat{f_Q}$ for the field galaxies within this redshift range. Blue squares denote the galaxies from Presotto et al. (2012), while the green diamonds denote the galaxies from Jian et al. (2017). The radial trend suggests that the probability of being quenched slowly increases with the time galaxies spend in groups, indicative of a slow quenching process.

To ensure our models best reflect the trends in the data, we have chosen uninformative priors for a and b. To verify that our results were not sensitive to small changes, in these priors we performed a sensitivity analysis considering a range of normal priors (mean from -5 to 5 and standard deviation from 1 to 10). This analysis shows that, unless a very small standard deviation for the priors is used, the resulting posterior does not change substantially. Therefore, our results are not significantly dependent on changes to the chosen priors.

In the sidebar of Figure 5 we define $\widehat{f_Q}$ to provide a general estimate of f_Q averaged over the redshift bin, radius from group center, and stellar mass. We define $\widehat{f_Q}$ as the number of quenched galaxies (n_q) divided by the total number of galaxies (n_T) in that bin. To calculate the error on $\widehat{f_Q}$ we use Bayes's theorem. Assuming that the likelihood of observing n_Q quenched galaxies out of a sample of n_T is binomial with probability $p = \widehat{f_Q}$ of a galaxy being quenched with $k = n_q$ successes and $n = n_T$ trials, the natural choice for a prior is a beta distribution with parameters $\alpha = \beta = 1$. In each considered bin, we report the maximum a posteriori value of $\widehat{f_Q}$ and the 68% confidence interval:

$$\text{Beta}(\alpha, \beta) \propto x^{\alpha-1}(1-x)^{\beta-1}, \quad (3)$$

$$\text{Binom}(k, n, p) \propto p^k(1-p)^{n+k}. \quad (4)$$

4. Results

For a rough understanding of the timescale of evolution for f_Q of group and field galaxies we look at the redshift evolution of f_Q in Figure 4. In this figure we show the redshift evolution of the quenched fraction of galaxies with a stellar mass greater than $10^{10.56}$ $M_\odot$ and with absolute B-band magnitude $M_B < -19.5–1.1z$. The pink and blue dashed lines show the Bayesian estimate of f_Q together with with the 68% confidence interval. The trend of the field is plotted in a blue dashed line, while the trend of the groups is plotted in a solid pink line. The top panel displays the distribution of field and group galaxies in redshift space. We find that f_Q for group galaxies increases as redshift decreases, from $0.59^{+0.13}_{-0.08}$ at $z = 0.8$ to $0.82^{+0.09}_{-0.10}$ at $z = 0.2$. For field galaxies, our results suggest that the quenched fraction remains relatively constant as a function of redshift, with f_Q varying between $0.05^{+0.08}_{-0.08}$ and $0.59^{+0.11}_{-0.10}$. This result is in agreement with values reported in the literature (e.g., Peng et al. 2010; Presotto et al. 2012; Knobel et al. 2013; Ji et al. 2018; Donnari et al. 2020). For example, Presotto et al. (2012) find that the fraction of quenched galaxies among massive objects in groups increases from $0.8^{+0.03}_{-0.03}$ to $0.86^{+0.03}_{-0.03}$ between redshifts 0.65 and 0.3, respectively.

Figure 4 shows that the difference between field and group galaxies becomes stronger as redshift decreases. The overall trend of the group galaxies compared to the stagnant field suggests the group environment significantly influences a galaxy's probability of being quenched. This influence either occurs the longer a galaxy is in a group or in groups that have formed at redshifts around 0.325.

The distributions of group and field galaxies illustrated in Figure 4 are only separated at lower redshifts and only by a small amount. To verify if these field and group distributions are unique, we perform three Anderson–Darling tests. The first test is over the entire redshift range; the second and third are over the higher- ($0.45 < z < 0.8$) and lower- ($0.2 < z < 0.45$) redshift ranges to see how the difference between the group and field distributions changes over time. The p-value of the Anderson–Darling test over the entire redshift range is 0.08. Typically two distributions are only considered significantly different if the p-value is less than 0.05, indicating that over the entire redshift range the two distributions could be drawn from

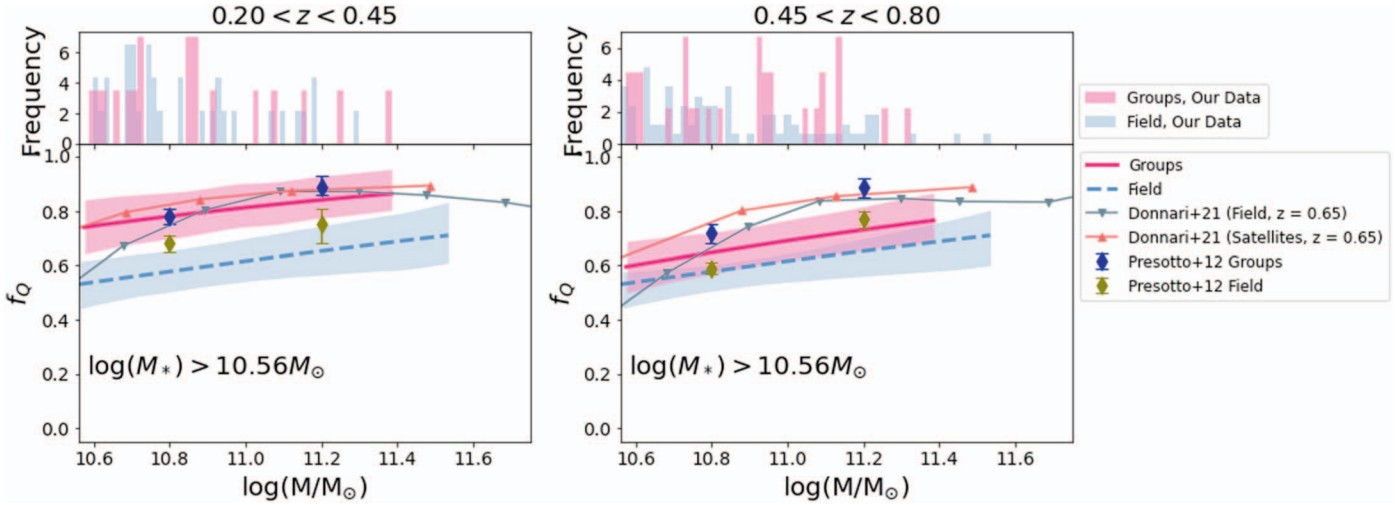

Figure 6. The bottom panels show the probability of being quenched (f_Q) derived from a logistic regression model vs. the stellar mass of the galaxies. The solid red line corresponds to the group galaxies, while the blue dashed line corresponds to the field galaxies. The left panel (top and bottom) is galaxies within the $0.2 < z < 0.45$ range, the right panel (top and bottom) is galaxies within the $0.45 < z < 0.8$ range; both are limited to $\log(M_*/M_\odot) \geqslant 10.56$ and $M_B < -19.5–1.1z$. The shaded regions are the 68th and 95th percentiles from the regression models. Quenched galaxies and star-forming galaxies are plotted as 1 and 0, respectively. The top two panels are weighted histograms of the group and field mass distributions, weighted so the area under their histograms integrates to 1. Upside-down gray triangles denote the simulated field values from Donnari et al. (2020), while the orange triangles denote the simulated satellite galaxies from Donnari et al. (2020). The blue diamonds indicate the group values from Presotto et al. (2012), while the green diamonds denote the field values from Presotto et al. (2012). Both bottom panels show that galaxies of higher stellar masses are more likely to undergo quenching. However, the effects of the environment become more apparent in the bottom left panel, where the f_Q exhibits a clearly different trend between the field and group galaxies. We also see in the top panels that the mass distribution of group and field galaxies are similar.

the same sample. The p-value of the higher-redshift range is >0.25, indicating the two distributions are likely drawn from the same distribution. The p-value in the lower-redshift range is 0.02, meaning in the lower-redshift range the two distributions are confidently different. What these Anderson–Darling tests tell us is that while the field and group distributions do not confidently differ over the entire redshift range, they begin to differ significantly at lower redshifts.

To investigate the timescale of environmental quenching within each redshift bin we explore the radial dependence of f_Q in Figure 5. We present the Bayesian estimate of f_Q, with the 68% interval, as a function of the distance to the group center ($r/r_{\rm gr}$) normalized by the radius of the group ($r_{\rm gr}$), derived in K12. The histogram indicates the radial distance distribution of galaxies used to derive the model. Finally, in the sidebar, we show the value of $\widehat{f_Q}$ for field galaxies.

Although the uncertainties are large, we do see a general radial dependence of f_Q. In the outskirt of groups, $f_Q = 0.40^{+0.13}_{-0.08}$, consistent with the average value measured in field galaxies ($f_Q = 0.52^{+0.08}_{-0.08}$) in the same redshift bin. Moving toward the central parts of groups, f_Q increases, reaching values of $f_Q = 0.86^{+0.09}_{-0.10}$. When interpreting this trend we must be careful, as beyond $r/r_{\rm gr} = 0.6$ we only have two points constraining our fit, which must be considered when we present our analysis in Section 3. However, the general trend indicates that the probability of being quenched is loosely dependent on the distance a galaxy is to its group center.

Figure 5 only includes the lower-redshift bin as the upper bin of $0.45 < z < 0.8$ is subject to differing uncertainties that make its interpretation difficult. We analyze the radial trend of f_Q with the assumption that $r/r_{\rm gr}$ is statistically correlated with the time since infall (Gao et al. 2004; Taranu et al. 2014). With the increased likelihood of nonvirialized halos and contamination at higher redshifts, this assumption breaks down. So we do not analyze the radial trend of f_Q in the $0.45 < z < 0.8$ redshift bin.

To explore the possibility of the trend in Figure 5 being driven by mass quenching, in Figure 6 we investigate how the probability of being quenched changes with galaxy stellar mass. As in the previous figures, we show the logistic regression of f_Q and the corresponding 68% confidence intervals. The low- and high-redshift bins are shown on the left and right panels, respectively. The top panel in each shows the mass distributions of galaxies in groups and in the field.

The probability of being quenched depends in similar ways on the stellar mass for group and field galaxies for the $0.45 < z < 0.8$ redshift range. Specifically, f_Q increases with increasing stellar mass among the group and field galaxies equally. This trend changes in the $0.2 < z < 0.45$ redshift range, where f_Q is similarly dependent on mass in the field but seems independent of mass in groups. We find that in this lower-redshift range the mass dependence of the groups and field are confidently different, with an Anderson–Darling p-value of 0.017. These relationships are in relative agreement with the literature (Presotto et al. 2012; Wetzel et al. 2013; Ji et al. 2018) with our values of f_Q being within the standard deviation of their results.

Due to the mass dependence of f_Q, its radial and redshift dependencies could be introduced if the mass distribution changes as a function of distance from the center of the group. We have tested this possibility and found that, at all redshifts, there is no correlation between a galaxy's stellar mass and the distance to its group's center or its redshift.

We have refrained from analyzing the relationship between f_Q and the group halo mass due to the size of our group sample. We have a total of eight groups in our lower-redshift sample and 12 in our higher-redshift sample. We do not believe that we can conduct a robust analysis on how f_Q changes with just the group halo mass. In an effort to marginalize over the effects that the group halo mass has on our results, we have included

the group halo mass in our model, plotted in Figure 5, where we have marginalized over the group halo mass.

5. Discussion

We begin the discussion of the results presented in the previous sections by addressing possible sources of systematic uncertainties, including comparison with different techniques used in similar studies in the literature and then discuss the quenching timescales.

5.1. Systematic Uncertainties

The UVCANDELS data set covers only approximately 4% of the COSMOS field used in K12, limiting the number of groups for which the new UV data is available. Small number statistics could then cause some of the trends we observe as well as add uncertainty in the measured values. However, the relative agreement that we observe between our trends and those resulting from larger samples of Presotto et al. (2012) and Ji et al. (2018) suggests that the effect of small number statistics is limited to increasing the uncertainties in the results and does not drive the trends we observed.

Another source of systematic uncertainty is caused by our selection method of quenched galaxies. It has been shown that the strategy used to identify the sample of quiescent galaxies can introduce significant differences in the measured values of f_Q, particularly for massive galaxies, with $\log(M_*/M_\odot) > 10.5$ (Donnari et al. 2021). We therefore explored how our choice of using the *UVJ* diagram, as opposed to other definitions in the literature, influences our results. To test the severity of this effect, we compare three definitions of quiescence. Specifically, we compare the *UVJ* methods from Williams et al. (2009) and this work, the rest-frame $U-B$ versus stellar mass method used in Presotto et al. (2012), as well as two differing sSFR (SFR/Stellar Mass) thresholds from Jian et al. (2017) and Donnari et al. (2020). We find that using either the two *UVJ* methods or the Donnari et al. (2020) sSFR method does not change the redshift evolution of the group and field galaxies significantly or the radial trend of f_Q. However, we find that using the methods from Presotto et al. (2012) and Jian et al. (2017) gives us significantly differing redshift evolutions and radial trends of f_Q. We believe that the sSFR threshold definition in Jian et al. (2017) is too high and allows for star-forming galaxies to contaminate the quiescent population at high masses. This is due to the turnoff of the SFR–M_* main sequence (Speagle et al. 2014), where galaxies with a lower sSFR are still characterized as star forming. The *U–B* versus stellar mass definition used in Presotto et al. (2012) also suffers from a contaminated quiescent population. We find that this method fails to completely disentangle dusty star-forming galaxies from quiescent galaxies, unlike the *UVJ* method used here and in Williams et al. (2009). While contamination is always likely with any definition of quiescence, we believe that the robustness of our measurements when using our *UVJ* definition, that of Williams et al. (2009), and the sSFR definition of Donnari et al. (2020) suggests we have minimized the contamination in our sample.

Presotto et al. (2012) studied the entire 20 k zCOSMOS group catalog, with similar mass, luminosity, and redshift cuts as we placed on our data. While they did not focus on the dominant quenching mechanism, they found similar radial trends and redshift evolution of f_Q. Their values of f_Q are consistently higher than what we find. This difference can be explained by their adopted selection of quenched galaxies. Specifically, they define quiescence using the $U-B$ versus stellar mass diagram. As Figure 2 shows, a cut based on only one color will result in a sample that includes star-forming, dusty galaxies, increasing the measured f_Q. Despite the value of f_Q being larger, however, the observed trends with redshift and group properties are similar to those we find here (see, e.g., Figure 4).

Another recent work addressing the evolution of the quenched fraction as a function of environment is Jian et al. (2017), who use the Pan-STARRS1 medium-deep survey (Kaiser et al. 2010) and focus on the same redshift range as our analysis. Their quenched fraction is higher than our values, in this case because the sSFR threshold they use in their analysis ($10^{-10.1}$ yr^{-1}) includes galaxies that we consider star forming (e.g., Figure 2). Furthermore their analysis is dependent on the radial trend of high-mass galaxies, where the contamination of star-forming galaxies becomes even more critical due to the turnoff of the SFR–M_* main sequence. However, comparisons with their radial trends are not ideal as they do not provide normalized distances to the group center nor the group radii themselves. To allow for any comparison we normalize their radial distances by 1.5 Mpc, which they quote as the average radius of their groups. It is because of these reasons that while our results are within agreement of their own, we come to differing conclusions as our analysis is not contaminated by star-forming galaxies to the extent that theirs is.

An additional uncertainty can be introduced by the assumption that the group dark matter halos are fully virialized. This assumption is used in the creation of the group catalog by K12, but it also enters in the analysis below when we link the group–center distance to the time since infall. This assumption may break for the highest redshift bin considered ($z > 0.45$). Groups' halos not being fully virialized could introduce an ambiguity in the definition of their radii, possibly resulting in incomplete (galaxies that are entering the group would be missed by our selection) and contaminated group catalogs (Alpaslan et al. 2012). However, we expect this problem to be minimized in our analysis as we limit our sample to groups with the highest-estimated purity and completeness.

5.2. Quenching Processes

Environmental quenching processes can be broadly separated into rapid and slow mechanisms depending on whether they remove the entirety of the cold material in a galaxy or only act on the outermost, low-density gas. In Section 4 we presented how the probability of being quenched (f_Q) for group galaxies depends on redshift, distance to the group center, and stellar mass. Here we analyze these trends to try and determine whether environmental quenching in groups is dominated by a slow or rapid mechanism.

Figure 4 shows that the redshift evolution of f_Q evolves differently for galaxies in groups than in the field. The gradual deviation between group and field galaxies suggests that the dominant quenching process in these groups is slow. If the dominant process is rapid, then we expect f_Q in groups to significantly differ from the field at all redshifts. Seeing the redshift evolution gradually diverge suggests that a majority of group galaxies are quenched only after several billion years after their accretion into a group. Direct interpretation of the redshift dependency of f_Q, however, can be blurred by the fact

that groups continue to accrete galaxies from the field environment, thus mixing together the quenching and accretion processes. This effect would be more important for slow quenching mechanisms (acting on timescales similar to those of accreting new galaxies) and minimized for rapid mechanisms (of the order of few Myr, e.g., for ram-pressure stripping).

A clearer picture of the influence of the group environment on quenching can be obtained by also looking at the distribution of f_Q as a function of how long group galaxies have been in groups. This can be done by examining the radial dependence of f_Q because the projected distance to the group center ($r/r_{\rm gr}$) is found to statistically correlate with the time since a galaxy's infall in the group halo. Numerical simulations show that the infall look-back time slowly declines with $r/r_{\rm gr}$, indicating that, statistically, galaxies projected closer to the center of groups have been in the group for a longer time (Gao et al. 2004; Taranu et al. 2014).

With this in mind, Figure 4 shows that, in the lower-redshift bin,[26] the longer a galaxy has been inside a group, the more likely it is to be quenched, confirming that the group environment influences the probability of being quenched. Interpreting this result in terms of quenching processes becomes difficult due to the low number of points constraining the outer values of our fit. If we observe the trend starting a $r/r_{\rm gr} \leqslant 0.6$, where we are more constrained, we see that f_Q is still within agreement of the field galaxies. This suggests that even when galaxies have been in a group for >1 Gyr their likelihood of being quenched is consistent with that of a field galaxy. Combined with the slow redshift evolution, this radial trend suggests that the dominant environmental quenching process acts on timescales of several billion years.

We emphasize that while our best estimate for the timescale of environmental quenching is long, implying a slow quenching process, more data are needed to confirm this result. Indeed, while the best fit of our models were used to conduct the analysis, the standard deviation is large, and thus we cannot completely rule out rapid quenching as a dominant mechanism in groups.

To quantify the quenching timescale (t_Q) of our lower-redshift bin, we follow the work of Foltz et al. (2018), who proposed a method for determining t_Q based on connecting the dark matter mass accretion rates to the observed numbers of quenched and star-forming galaxies. To briefly summarize, we first define the mass accretion rate of the group dark matter halo:

$$\frac{dM}{dt} = 46.1 \mathrm{M}_{\odot}\mathrm{yr}^{-1}\left(\frac{M}{10^{12}M_{\odot}}\right)^{1.1} * (1 + 1.11z)\sqrt{\Omega_m(1+z)^3 + \Omega_\lambda}, \quad (5)$$

$$M(z_c) = M_0, \quad (6)$$

where M is the mass of the group dark matter halo, M_0 is the observed mass of the halo (calculated in K12), Ω_m is the matter overdensity of the universe, and Ω_λ is the dark energy overdensity of the universe. To solve this differential equation, we use the observed redshift z_c and mass M_0 of a given group as the initial value. To solve for the quenching time, we assume that all star-forming galaxies (B) have been in their group for less than the quenching time, while all quenched (R) galaxies have been in the group for at least the quenching time. From this we can relate the ratio of B and R to the ratio of the group dark matter halo mass at the time it is observed ($M(z_c)$) and one quenching time before it was observed ($M(z_c + \Delta z_Q)$):

$$\frac{B}{R} = \frac{M(z_c) - M(z_c + \Delta z_Q)}{M(z_c + \Delta z_Q)} \quad (7)$$

For a more detailed explanation of the reasoning we direct the reader's attention to Appendix B of Foltz et al. (2018).

To calculate the error on our derived t_Q, we use a Monte Carlo simulation where we vary the ratio of B and R as well as z_c and M_0. In each realization of the simulation we select z_c and M_0 from the distribution of group dark matter halo masses in our sample. We also derive B/R from the distribution of $\widehat{f_Q}$ for the group galaxies in this redshift range. We use the spread of the resulting t_Q distribution as an estimate of the systematic uncertainty associated with t_Q. We find a quenching timescale $t_Q = 4.91^{+0.91}_{-1.47}$ Gyr. This method, however, assumes a slow timescale and depends on the exact value of f_Q, which, in turn, as we showed in the previous section, depends on the definition used to select quenched galaxies.

6. Conclusions

We use a sample of 20 groups from the zCOSMOS 20 k group catalog in the redshift range of $0.2 < z < 0.8$ to study the dominant method of environmental quenching in galaxy groups. We added new UV data from UVCANDELS to existing multiband photometry to derive galaxy physical properties.

We identify quenched galaxies using the *UVJ* diagram and explore the probability of being quenched (f_Q) in groups and the field as a function of redshift, stellar mass, and time within a group. Limiting the analysis to galaxies with $\log(M_*/M_{\odot}) > 10.56$, we find that f_Q changes slowly with redshift, from $0.59^{+0.13}_{-0.08}$ at $z = 0.8$ to $0.82^{+0.09}_{-0.10}$ at $z = 0.2$, compared to field galaxies, where f_Q remains constant around $0.59^{+0.11}_{-0.10}$ from $z = 0.8$ to $z = 0.2$. We find that f_Q decreases as a function of distance to the group center in the lower-redshift bin, suggesting that the longer a galaxy has been in a group, the higher the probability of it being quenched. Combining the radial trend of f_Q and the redshift evolution of f_Q suggests that the dominant environmental quenching mechanism in our sample is a slow process, such as strangulation (Larson et al. 1980) or delayed then rapid (Wetzel et al. 2013). Assuming the quenching process is slow, we used the fraction of quenched galaxies to compute quenching timescales of $t_Q = 4.91^{+0.91}_{-1.47}$ Gyr. This number, however, is highly uncertain because of the assumed halo mass accretion rate and its dependency on the definition of quenched galaxies.

In future work, we plan to extend the analysis of the impact of group environment on galactic star formation to the remaining three fields that are covered by the UVCANDELS survey. The UV and *B*-band data available in this survey allow for improved photometric redshift quality and thus have a more robust field sample. Future exploration of a wider array of environments such as with the upcoming Euclid Space Telescope, Nancy Grace Roman Space Telescope, and recently launched JWST will help further constrain the role of the environment within groups. Fields such as COSMOS, with the wide array of band coverage, create a unique data set to study these environmental effects, and future UV projects in this field

[26] We refrain from commenting on the high-redshift bin because, as we discussed in 5.1, we believe that these groups are more likely to not yet be fully virialized.

would offer even further constraints on the vital role of environment on extragalactic evolution.

Based on observations with the NASA/ESA/CSA Hubble Space Telescope obtained at the Space Telescope Science Institute, which is operated by the Association of Universities for Research in Astronomy, Incorporated, under NASA contract NAS5-26555. Support for Program number 15647 was provided through a grant from the STScI under NASA contract NAS5-26555.

Y.S.D. acknowledges the support from National Key R&D Program of China for grant No. 2022YFA1605000, and the NSFC grants Nos. 12273051 and 11933003.

L.Y.A.Y. is supported by an appointment to the NASA Postdoctoral Program (NPP) at NASA Goddard Space Flight Center, administered by Oak Ridge Associated Universities under contract with NASA.

R.A.W. acknowledges support from NASA JWST Interdisciplinary Scientist grants NAG5-12460, NNX14AN10G and 80NSSC18K0200 from GSFC.

Special thanks to Prof. Galin Jones for helping us revise our statistical analysis.

ORCID iDs

Maxwell Kuschel https://orcid.org/0000-0002-7830-363X
Claudia Scarlata https://orcid.org/0000-0002-9136-8876
Vihang Mehta https://orcid.org/0000-0001-7166-6035
Harry I. Teplitz https://orcid.org/0000-0002-7064-5424
Marc Rafelski https://orcid.org/0000-0002-9946-4731
Xin Wang https://orcid.org/0000-0002-9373-3865
Ben Sunnquist https://orcid.org/0000-0003-3759-8707
Laura Prichard https://orcid.org/0000-0002-0604-654X
Norman Grogin https://orcid.org/0000-0001-9440-8872
Anton Koekemoer https://orcid.org/0000-0002-6610-2048
Rogier Windhorst https://orcid.org/0000-0001-8156-6281
Michael Rutkowski https://orcid.org/0000-0001-7016-5220
Anahita Alavi https://orcid.org/0000-0002-8630-6435
Nima Chartab https://orcid.org/0000-0003-3691-937X
Christopher J. Conselice https://orcid.org/0000-0003-1949-7638
Y. Sophia Dai https://orcid.org/0000-0002-7928-416X
Eric Gawiser https://orcid.org/0000-0003-1530-8713
Mauro Giavalisco https://orcid.org/0000-0002-7831-8751
Pablo Arrabal Haro https://orcid.org/0000-0002-7959-8783
Nimish Hathi https://orcid.org/0000-0001-6145-5090
Rolf A. Jansen https://orcid.org/0000-0003-1268-5230
Zhiyuan Ji https://orcid.org/0000-0001-7673-2257
Ray A. Lucas https://orcid.org/0000-0003-1581-7825
Robert W. O'Connell https://orcid.org/0000-0002-8190-7573
Brant Robertson https://orcid.org/0000-0002-4271-0364
Zahra Sattari https://orcid.org/0000-0002-0364-1159
L. Y. Aaron Yung https://orcid.org/0000-0003-3466-035X
Romeel Davé https://orcid.org/0000-0003-2842-9434
Duilia DeMello https://orcid.org/0000-0003-1624-8425
Mark Dickinson https://orcid.org/0000-0001-5414-5131
Henry Ferguson https://orcid.org/0000-0001-7113-2738
Steven L. Finkelstein https://orcid.org/0000-0001-8519-1130
Matt Hayes https://orcid.org/0000-0001-8587-218X
Justin Howell https://orcid.org/0000-0002-5924-0629
Sugata Kaviraj https://orcid.org/0000-0002-5601-575X
John W. Mackenty https://orcid.org/0000-0001-6529-8416
Brian Siana https://orcid.org/0000-0002-4935-9511

References

Alpaslan, M., Robotham, A. S. G., Driver, S., et al. 2012, MNRAS, 426, 2832
Berlind, A. A., Frieman, J. A., Weinberg, D. H., et al. 2006, ApJS, 167, 1
Boquien, M., Burgarella, D., Roehlly, Y., et al. 2019, A&A, 622, A103
Brammer, G. B., Whitaker, K. E., van Dokkum, P. G. v., et al. 2011, ApJ, 739, 24
Bruzual, G., & Charlot, S. 2003, MNRAS, 344, 1000
Burgarella, D., Buat, V., & Iglesias-Paramo, J. 2005, MNRAS, 360, 1413
Chabrier, G. 2003, PASP, 115, 763
Charlot, S., & Fall, S. M. 2000, ApJ, 539, 718
Donnari, M., Pillepich, A., Nelson, D., et al. 2021, MNRAS, 506, 4760
Donnari, M., Pillepich, A., Joshi, G. D., et al. 2020, MNRAS, 500, 4004
Eke, V. R., Frenk, C. S., Baugh, C. M., et al. 2004, MNRAS, 355, 769
Foltz, R., Wilson, G., Muzzin, A., et al. 2018, ApJ, 866, 136
Ford, A. B., Werk, J. K., Dave, R., et al. 2016, MNRAS, 459, 1745
Gao, L., White, S. D. M., Jenkins, A., Stoehr, F., & Springel, V. 2004, MNRAS, 355, 819
Gray, R., Messenger, C., & Veitch, J. 2022, MNRAS, 512, 1127
Grogin, N. A., Kocevski, D. D., Faber, S. M., et al. 2011, ApJS, 197, 35
Gunn, J. E., & Gott, J. R. I. 1972, ApJ, 176, 1
He, Z., Wang, T., Liu, G., et al. 2019, NatAs, 3, 265
Huchra, J. P., & Geller, M. J. 1982, ApJ, 257, 423
Iovino, A., Cucciati, O., Scodeggio, M., et al. 2010, A&A, 509, A40
Jeans, J. H. 1902, RSPTA, 199, 1
Ji, Z., Giavalisco, M., Williams, C. C., et al. 2018, ApJ, 862, 135
Jian, H.-Y., Lin, L., Lin, K.-Y., et al. 2017, ApJ, 845, 74
Kaiser, N., Burgett, W., Chambers, K., et al. 2010, Proc. SPIE, 7733, 77330E
Kawata, D., & Mulchaey, J. S. 2008, ApJL, 672, L103
Kitzbichler, M. G., & White, S. D. M. 2007, MNRAS, 376, 2
Knobel, C., Lilly, S. J., Iovino, A., et al. 2009, ApJ, 697, 1842
Knobel, C., Lilly, S. J., Iovino, A., et al. 2012, ApJ, 753, 121
Knobel, C., Lilly, S. J., Kovac, K., et al. 2013, ApJ, 769, 24
Koekemoer, A. M., Faber, S. M., Ferguson, H. C., et al. 2011, ApJS, 197, 36
Larson, R. B. 1972, Natur, 236, 21
Larson, R. B., Tinsley, B. M., & Caldwell, C. N. 1980, ApJ, 237, 692
Lilly, S. J., Carollo, C. M., Pipino, A., Renzini, A., & Peng, Y. 2013, ApJ, 772, 119
Lilly, S. J., Le Brun, V., Maier, C., et al. 2009, ApJS, 184, 218
Martig, M., Bournaud, F., Teyssier, R., & Dekel, A. 2009, ApJ, 707, 250
Martis, N. S., Marchesini, D., Brammer, G. B., et al. 2016, ApJL, 827, L25
McPartland, C., Ebeling, H., Roediger, E., & Blumenthal, K. 2016, MNRAS, 455, 2994
Moore, B., Katz, N., Lake, G., Dressler, A., & Oemler, A. 1996, Natur, 379, 613
Murray, N., Menard, B., & Thompson, T. A. 2011, ApJ, 735, 66
Muzzin, A., Marchesini, D., Stefanon, M., et al. 2013, ApJ, 777, 18
Nayyeri, H., Hemmati, S., Mobasher, B., et al. 2017, ApJS, 228, 7
Noll, S., Burgarella, D., Giovannoli, E., et al. 2009, A&A, 507, 1793
Oke, J. B. 1974, ApJS, 27, 21
Oosterloo, T., Morganti, R., & Sadler, E. M. 2001, in ASP Conf. Proc. 240, Gas and Galaxy Evolution (San Francisco, CA: ASP), 251
Peng, Y.-j., Lilly, S. J., Kovac, K., et al. 2010, ApJ, 721, 193
Planck Collaboration, Aghanim, N., Akrami, Y., et al. 2020, A&A, 641, A6
Presotto, V., Iovino, A., Scodeggio, M., et al. 2012, A&A, 539, A55
Rafelski, M., Teplitz, H. I., Gardner, J. P., et al. 2015, AJ, 150, 31
Salvatier, J., Wieckia, T. V., & Fonnesbeck, C. 2016, PyMC3: Python probabilistic programming framework, Astrophysics Source Code Library, ascl:1610.016
Speagle, J. S., Steinhardt, C. L., Capak, P. L., & Silverman, J. D. 2014, ApJS, 214, 15
Springel, V., White, S. D. M., Jenkins, A., et al. 2005, Natur, 435, 629
Taranu, D. S., Hudson, M. J., Balogh, M. L., et al. 2014, MNRAS, 440, 1934
Wagner, C. R., Courteau, S., Brodwin, M., et al. 2016, ApJ, 834, 53
Werk, J. K., Prochaska, J. X., Cantalupo, S., et al. 2016, ApJ, 833, 54
Wetzel, A. R., Tinker, J. L., Conroy, C., & van den Bosch, F. C. v. 2013, MNRAS, 432, 336
Whitaker, K. E., van Dokkum, P. G., Brammer, G., & Franx, M. 2012, ApJL, 754, L29
Whitaker, K. E., Labbé, I., Dokkum, P. G. v., et al. 2011, ApJ, 735, 86
Whitaker, K. E., Franx, M., Bezanson, R., et al. 2015, ApJL, 811, L12
Williams, R. J., Quadri, R. F., Franx, M., van Dokkum, P., & Labbe, I. 2009, ApJ, 691, 1879
Zucca, E., Bardelli, S., Bolzonella, M., et al. 2009, A&A, 508 1217